ELSEVIER

Journal of Atmospheric and Solar-Terrestrial Physics 69 (2007) 1657–1667

Journal of ATMOSPHERIC AND SOLAR-TERRESTRIAL PHYSICS

www.elsevier.com/locate/jastp

The effective altitude range of the ionospheric Alfvén resonator studied by high-altitude EISCAT measurements

K. Prikner[a,*], K. Mursula[b,**], T. Bösinger[b], F.Z. Feygin[c], T. Raita[d]

[a]*Geophysical Institute, Academy of Sciences of the Czech Republic, Boční II/1401, 14131 Praha 4-Spořilov, Czech Republic*
[b]*Department of Physical Sciences, University of Oulu, PO Box 3000, 90014 Oulu, Finland*
[c]*United Institute of Physics of the Earth, Russian Academy of Sciences, Bolshaya Gruzinskaya 10, 123995 Moscow, Russian Federation*
[d]*Sodankylä Geophysical Observatory, University of Oulu, 99600 Sodankylä, Finland*

Received 14 June 2006; received in revised form 23 October 2006; accepted 10 November 2006
Available online 12 July 2007

Abstract

The altitude profiles of ionospheric plasma obtained by the EISCAT incoherent scatter radar can be used to study the effect of the ionospheric Alfvén resonator (IAR) upon the formation of the wave signal on the ground. We examine here a fortunate case of a multiband wave Pc1 event on March 7, 2001, at a time when the EISCAT radar was operated in two modes simultaneously, thus covering an exceptionally wide altitude range. This made it possible to test the IAR model and its effect upon the wave signal over a larger altitude range than earlier, and to determine the effective altitude range of the resonator (the IAR domain), which has to be taken into account in full-wave numerical modeling. This case study demonstrates that the IAR domain that affects the wave signal on the ground is essentially localized below the height of about 1200–1500 km.

Keywords: Ionospheric Alfvén resonator; Subauroral Pc1 pulsations; Numerical simulation; Resonator domain; EISCAT data

1. Introduction

We have studied earlier a subauroral multiband Pc1 wave event in terms the effect of the ionospheric Alfvén resonator (IAR) on the wave signal, using full-wave numerical modeling (Prikner et al., 2004). Other, more traditional approaches to explain the generation of multiband Pc1 events include the ionospheric waveguide ducting of waves from multiple sources (Greifinger and Greifinger, 1968) and the spectral splitting of waves due to magnetospheric heavy ions He^+ and O^+ (Young et al., 1981; Kozyra et al., 1984).

The so-called spectral resonance structures (SRS), observed from high to low latitudes (see, e.g., Bösinger et al., 2002, 2004; Hebden et al., 2005), are a special type of multiband wave events. The SRS events provide definite evidence for the existence and harmonic structure of the IAR in terms of its effect on the electromagnetic background noise. The SRS structures are usually seen in the frequency range between 0.1 and 6 Hz.

Feygin et al. (1994) studied coherent multiple Pc1 pulsation bands recorded at Finnish stations,

*Corresponding author. Tel.: +420 2 67103354; fax: +420 2 72761549.
**Also for correspondence. Tel.: +358 8 5531366; fax: +358 8 5531287.
E-mail addresses: kpr@ig.cas.cz (K. Prikner), kalevi.mursula@oulu.fi (K. Mursula).

1364-6826/$ - see front matter © 2007 Published by Elsevier Ltd.
doi:10.1016/j.jastp.2006.11.005

suggesting that the central frequencies of the simultaneous Pc1 bands agree with the IAR resonance properties. On the other hand, the Pc1 pulsations and other forms of pulsations such as, e.g., IPDP (Prikner et al., 2002) typically occupy, especially at mid- to subauroral latitudes, frequencies that coincide with some of the lowest IAR harmonics in the frequency range between 0.2 and 3 Hz. The IAR acts as a band-pass filter for Pc1 waves (magnetospheric EMIC waves), modifying them and passing them to the ground preferably at the IAR eigenfrequencies, i.e., peaks of the transmission coefficient spectra. Note that the IAR is quite a low-Q resonator so that the signal on the ground is only modified, not completely determined by the IAR frequencies.

It is important to know what altitude range of the ionosphere (the so-called IAR domain) has to be taken into account when modeling the IAR in order to ensure a reliable model spectrum of the transmitted signal. In other words, what is the IAR domain that essentially forms the ground wave (e.g., multiband) signal? It is known that the most important part of the ionosphere for the IAR is localized around the F2 density maximum. The traditional view is the IAR domain extends up to the Alfvén velocity maximum, somewhere at an altitude of about 2000–3000 km. We have earlier used the CP-1 mode measurements of the EISCAT radar when modeling the IAR at high latitudes. However, the CP-1 measurements only extend to the altitude of 600 km. Thus, in order to be able to model reliably the IAR properties by the numerical full-wave code (Prikner and Vagner, 1991) we have had to extrapolate the ionosphere up to about 2000 km in altitude (Prikner et al., 2004; Prikner and Kerttula, 2005). The EISCAT radar operates several different modes, of which the so-called CP-7 experiment provides ionospheric plasma data at a wide range of altitudes, roughly between 300 and 2000 km. Luckily, the low-altitude CP-1 code and the wide-range CP-7 code measurements are sometimes operated simultaneously, thus giving comprehensive information of ionospheric plasma parameters through the entire vertical profile required for IAR modeling. Sometimes, although even more rarely, this occurs simultaneously with strong Pc1 waves.

In the present article, we study and make a numerical analysis for a multiband Pc1 wave event, making use of simultaneously operated EISCAT CP-1 and CP-7 mode measurements. We complete the EISCAT measurements by the International Reference Ionosphere (IRI) model on part of the plasma temperature profile. Using the EISCAT measurements of electron and ion density profiles ($N_e(z)$, the basic parameter for IAR eigenfrequencies) up to about 2300 km, we will study the effect of the IAR and the altitude range required to cover in order to guarantee reliable model results.

2. Observations

2.1. Wave dynamic spectra

Figs. 1a and b show the dynamic spectra of total power during a multiband pulsation event at Kilpisjärvi (KIL; 69.0° GG latitude, 20.9° GG longitude, 65.9° CGM latitude, 105.3° CGM longitude, $L = 6.0$) and Ivalo (IVA; 68.7° GG latitude, 27.3° GG longitude, 65.0° CGM latitude, 109.8° CGM longitude, $L = 5.6$) in northern Finland on 7 March 2001 from 08:30 to 15:00 UT (LT = UT + 2 h). The pulsation data are sampled at the rate of 40 samples/s and were FFT transformed for Fig. 1 using a spectral window size of 512 points. Both the EISCAT CP-1 and CP-7 modes were simultaneously operating during the time interval (to be called Interval I) between 08:45 and 11:00 UT, thus providing the entire vertical profile of the ionospheric density up to 2310 km in altitude. The temperature parameters were only available up to about 800 km. Thereafter, during the time to be called Interval II, between 11:00 and 13:00 UT, only the CP-7 mode was continued.

2.1.1. Interval I

As can be seen from Fig. 1, there is a persistent wave band at about 0.05–0.17 Hz, which continues throughout the whole time interval depicted in Fig. 1, with rather systematically decreasing amplitude. Moreover, during Interval I at about 09:15–10:40 UT another narrow wave band was registered, with the mean frequency slightly decreasing from about 0.65–0.50 Hz. This band was more intensive at IVA than at KIL, indicating that the source of the primary EMIC waves was likely at an L shell equatorward of KIL and closer to IVA. The frequencies of the two bands were practically identical at the two stations.

2.1.2. Interval II

After two short PiB-type bursts at about 11:00 and 11:10 UT, new, intensive waves appear at the

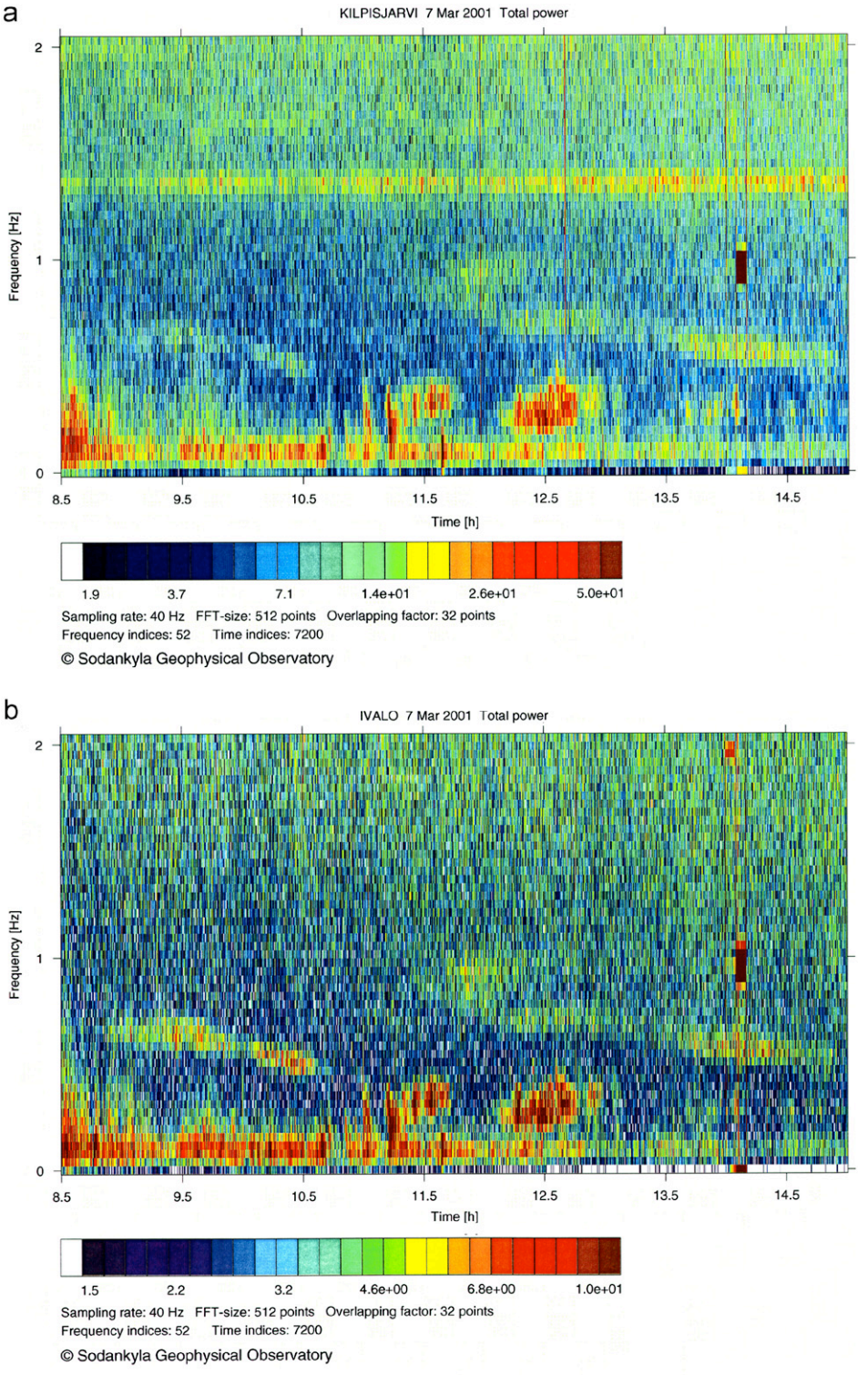

Fig. 1. Dynamic spectra of the total power of the magnetic H component during a multiband wave event in the Pc1 frequency range recorded at the (a) Kilpisjärvi (KIL) and (b) Ivalo (IVA) station on March 7, 2001 between 08:30 and 15:00 UT.

frequency of about 0.20–0.45 Hz. These waves do not form a continuous band but appear as three short sub-bands of about 30 min each. Two first sub-bands at about 11:15–11:45 UT and 12:15–12:45 UT are very strong but the third appears weakly at KIL only. There is some indication of a small increase of the mean frequency within the two first sub-bands. Also, especially the first sub-band depicts evidence for a pearl structure. At about 11:45 UT, another, rather weak high-frequency band appears at the frequency of about 0.75–1.00 Hz, which separates after 12:10 UT into two weak bands, one at about 0.64–0.75 Hz and the other at 0.90–1.00 Hz. As for Interval I, the frequencies of all bands are practically identical at the two stations.

2.2. EISCAT measurements and the IAR simulation model

The EISCAT radar was monitoring the high-latitude ionosphere above Tromsø from 08:45 to 13:00 UT, i.e., during most of the multiband Pc1 event. The radar was simultaneously operated in the CP-1 and CP-7 modes during Interval I up to 11:00 UT. From 11:00 to 13:00 UT (Interval II) only the CP-7 mode was used. Around the local noon (at KIL and IVA LT = UT + 2) the F2-layer density maximum may be considered relatively stable (stable K-indices during the whole time interval studied, $K = 2$ at Sodankylä). Moreover, the E-layer was found to be very stable throughout the studied interval, as shown by the EISCAT and ionogram data. Accordingly, the vertical profile up to the altitude of 300 km height (below the CP-7 mode range) can be taken to be constant so that the last CP-1 mode measurements at the end of Interval I may represent the vertical plasma profile in the lower ionosphere through the whole Interval II.

The radar beam was directed along the background magnetic field. Therefore the measurements correspond quite well to the ionospheric conditions above KIL, which is situated at the same latitude as Tromsø, only 2° more eastward. Fig. 2 illustrates the altitude profiles during the measurement at 12:35 UT up to the 2300 km altitude for the

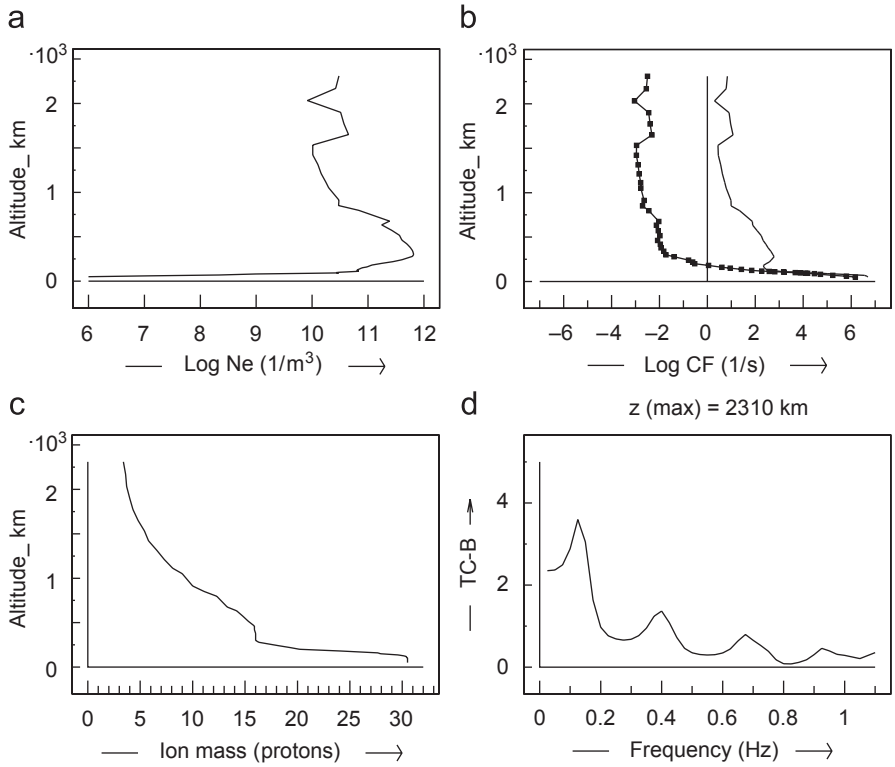

Fig. 2. Altitude profiles up to 2310 km of (a) the electron density, (b) electron (solid line) and ion (solid line with points) collision frequencies, (c) local effective ion mass in units of the proton mass. (d) Frequency spectrum of the transmission TC coefficient computed using EISCAT CP-1 and CP-7 mode measurements on March 7, 2001, at 12:35 UT.

following variables: (a) the electron density N_e, (b) the electron and ion collision frequencies modeled according to Prikner (1986) and Fatkullin et al. (1981), and (c) the effective ion mass. The electron and ion temperature parameters used to construct the profiles of Fig. 2b were extrapolated above the CP-7 temperature measurement range (i.e., above 700–800 km) by the IRI model.

As seen in Fig. 2c, up to the altitude of about 400 km heavy ions like O^+ dominate the ionospheric plasma density and their vertical density distribution plays a significant role in the formation of the IAR eigenfrequencies (Prikner and Kerttula, 2005). Higher up, the O^+ density decreases roughly exponentially and the light ions (H^+ and partly He^+) begin to dominate, contributing mainly to wave attenuation, but not so much to the resonator's harmonic frequencies (Prikner and Kerttula, 2005). Fig. 2a also shows rather abrupt variations of N_e (z) at altitudes above some 1500 km. These occur during the whole EISCAT CP-7 measurement interval and are likely related to the intrusion of light ions into the upper ionosphere.

The used full-wave numerical code is based on a 4×4 matrix method developed by Prikner and Vagner (1991). It allows one to estimate the frequency response of the ionospheric Alfvén resonator (wave $\boldsymbol{B}$- and $\boldsymbol{E}$-fields) on the ground as well as at any altitude level within the IAR. An Alfvenic (L-mode) plane wave of frequency f and wave vector $\boldsymbol{k}$ is assumed to be incident at the top of the ionosphere, which is taken as a vertically inhomogeneous (horizontally stratified), magnetoactive region with an external dipole field $\boldsymbol{B}_E$. A parallel incidence $\boldsymbol{k} \| \boldsymbol{B}_E$ is an acceptable assumption for IAR presentation.

The main input characteristics of the ionospheric medium are realistic altitude profiles of the electron-ion density $N_e(z)$ (quasi-neutral ionosphere is assumed), the effective ion mass of the plasma composition, and profiles of effective ion and electron collisions (see Prikner et al., 2001). The output characteristics are complex amplitudes of the total wave fields ($\boldsymbol{B}$, $\boldsymbol{E}$) of which the various wave characteristics, e.g., the amplitude transmission and reflection coefficients, can be determined.

The variables depicted in Figs. 2a–c are the basic input parameters for the full-wave numerical modeling already applied in our previous papers (see, e.g., Mursula et al., 2000; Prikner et al., 2001, 2004). The wave's (frequency f) transmission coefficient (TC) quantifies the transmission of the wave to the ground. For our purpose it is adequate to define it simply as the horizontal component of the wave's magnetic field amplitude on the ground (z_0) normalized by the incoming field amplitude:

$$\mathrm{TC}(f, z_0) = B_h(f, z_0)/B_h^{inc}(f, z_{max}), \quad (1)$$

where z_{max} is the ionospheric boundary of the incoming wave. We will also calculate the normalized magnetic amplitude at arbitrary altitude levels z:

$$\mathrm{TC}(f, z) = B_h(f, z)/B_h^{inc}(f, z_{max}). \quad (2)$$

The horizontal component of the wave's magnetic field is

$$B_h(f, z) = \sqrt{[|B_x(f, z)|^2 + |B_y(f, z)|^2]} \quad (3)$$

and B_x, B_y are the two complex horizontal components of the wave's magnetic field vector $\boldsymbol{B}(f, z)$.

An Alfvenic L-mode wave (parallel to the magnetic field line, $\boldsymbol{k} \| \boldsymbol{B}_E$) incident at the IAR upper boundary z_{max} was assumed for the model computation of the transmission coefficient TC (Eq. (1)). We take the angle of incidence (local inclination) at the boundary $z_{max} = 2310$ km (the maximum CP-7 altitude) to be $\vartheta_{\|} = 66^\circ$ corresponding to KIL and IVA stations. The ionosphere is presented as a stack of thin (10 km) and homogeneous planar layers from 50 km up to z_{max} permeated by an external dipole magnetic field with a moment $|\boldsymbol{M}_E| = 8.17 \times 10^{22}$ A m^2. Below the height 50 km the atmosphere is taken to be an insulator. The conductivity of the Earth's surface is assumed to be homogeneous with the specific value $\sigma_E = 10^{-2}$ s/m.

Fig. 2d shows the frequency dependence of the wave transmission coefficient TC(f) using the EISCAT measurements of the ionosphere at 12:35 UT. The IAR resonance peaks are displayed up to a frequency of about 1 Hz. Note that the resonance frequencies depend mainly on the vertical profiles of the electron and ion density and ion composition, while dissipation is controlled by conductivity, i.e. by ion density, ion collisions, and thus by the temperature profiles.

The peaks (local maxima) of TC correspond to the fundamental frequency $f_0 \approx 0.13$ Hz and the higher harmonics of $f_1 \approx 0.39$, $f_2 \approx 0.68$, and $f_3 \approx 0.93$ Hz, which are quite close to odd multiples of the fundamental (see, e.g., Cummings et al., 1969; Lysak, 1999). This property characterizes a quarter-wave type nature of the resonator. When comparing the resonance structure of Fig. 2d with the wave

pattern of Figs. 1a and 1b at 12:35 UT, the coincidence between the resonance peaks of TC(f) with the frequencies of the wave bands is evident.

3. IAR frequencies and IAR effective altitude range

3.1. The multiband wave event and the modeled IAR harmonics

We have calculated the TC(f) coefficients through the whole time interval of EISCAT measurements (08:45–13:00 UT) with the time resolution of 5 min. Fig. 3 displays the calculated peaks of TC(f) together with the frequency ranges of the wave bands observed at KIL (Fig. 3a) and IVA (Fig. 3b). (The calculations are the same for the two stations but the wave frequency ranges differ slightly.) The dots connected with lines indicate the calculated peak frequencies. The vertical bars indicate the frequency range of the wave bands recorded at the two stations (compare with Figs. 1a and b).

Comparing the calculated and observed frequencies in Fig. 3 during Interval I it is evident that the narrow EMIC wave band whose frequency decreases from about 0.65 to 0.50 Hz during the event agrees with the second harmonic f_2 of the IAR. The time series of calculated f_2 frequencies show considerable variation in time but also some simultaneous tendency for a decreasing mean frequency. Anyway, especially the stronger signal observed at IVA covers roughly the same range as the calculated f_2-peak during the event. The other signal seen during Interval I at a very low frequency of around 0.1 Hz agrees well with the calculated

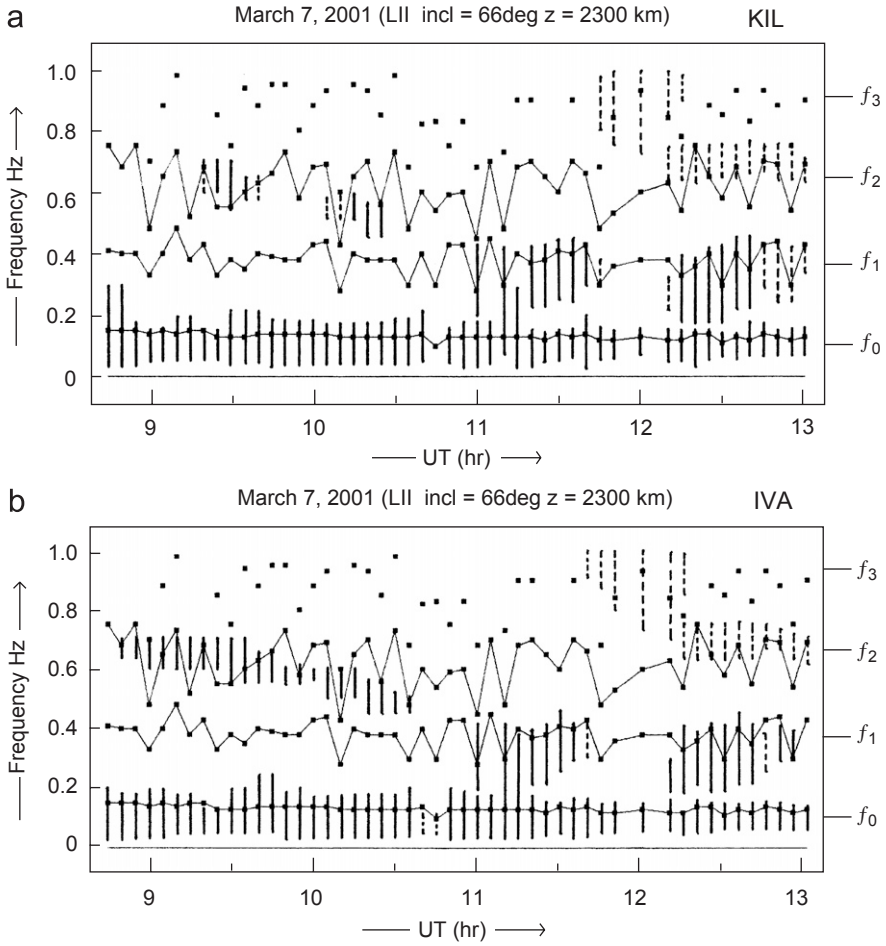

Fig. 3. Harmonic eigenfrequencies of the IAR resonator (maxima of the TC spectra) calculated every 5 min (squared dots with or without lines) and the frequency ranges of the wave bands (thick vertical bars) observed at (a) KIL and (b) IVA on March 7, 2001, between 08:45 and 13:00 UT.

fundamental frequency f_0. As noted above (see also Fig. 1), this band has a roughly constant frequency but a steadily decreasing amplitude. This wave band may have been ducted to the observation region from higher latitudes and its source may be the high-latitude, low-frequency EMIC waves or background noise in the form of PiC-type pulsations due to particle precipitation at higher latitudes. Even if this band did indeed come via the ionospheric duct, the local IAR properties would still affect it similarly as waves coming field-aligned. Therefore the agreement with the calculated f_0 frequency is no coincidence.

During Interval II, the frequency range of the strong, partly structured EMIC waves consisting of three sub-bands coincides well with the calculated frequency of the first IAR harmonic f_1. Here also the calculated frequencies vary considerably. The observed wave frequencies not only cover this range but even extend partly beyond this range, especially during the second sub-band where the variation of calculated frequencies is somewhat smaller. This shows that strong EMIC waves can be observed on the ground even at frequencies which do not correspond exactly to TC maxima, but they cover wide TC peak ranges where values $TC \geqslant 1$. In other words, the IAR is not a perfect but a rather low-Q resonator and filter. Moreover, the two weak higher-frequency bands that appear at about 12 UT seem to roughly coincide with the calculated second (f_2) and third (f_3) IAR harmonic.

3.2. Estimating the effective IAR domain

We have constructed an average model for the vertical profile of the ionosphere in order to estimate the effective altitude range of the IAR, i.e., the altitude region that has to be covered in order to achieve realistic results when modeling the IAR. We have averaged all the vertical profiles of plasma density and temperature between 11:00 and 13:00 UT when all the four wave bands with frequencies close to the four lowest IAR harmonics f_0–f_3 were observed. The vertical profile of the effective ion mass remains the same as in Fig. 2c. Fig. 4 depicts the averaged vertical profiles of (a) the electron-ion concentration $N_e(z)$ assuming a quasi-neutral plasma medium ($N_e \approx N_i$), (b) electron and ion collision frequencies, and (c) the Alfvén velocity. It is evident that averaging smoothes down the large variations of plasma density seen at high altitudes during the shorter time intervals (see

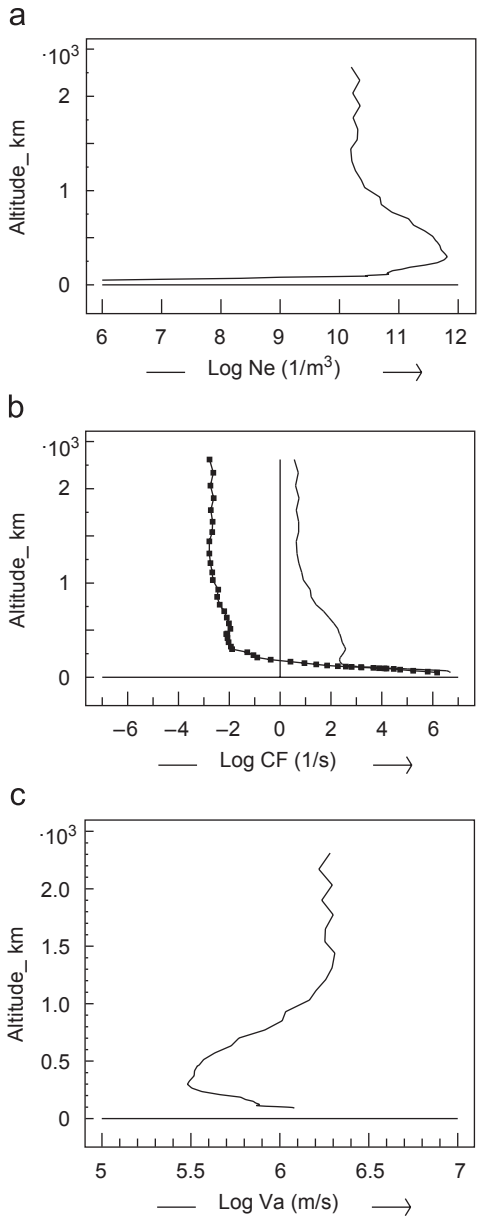

Fig. 4. Averaged altitude profiles of (a) the electron density, (b) electron (solid line) and ion (solid lines with points) collision frequencies, and (c) Alfvén velocity determined over the time interval 11:00–13:00 UT.

Fig. 2a). Also, the mean plasma density (predominating light ions) stays practically constant above the altitude of about 1500 km (see Fig. 2a). On the other hand, the density of heavy ions like O^+ decreases practically exponentially above the F2-layer maximum and can be neglected above 2000 km (see Fig. 2c; Prikner and Kerttula, 2005). The Alfvén velocity (Fig. 4c) reaches a local

maximum at about 1500 km and remains practically constant at higher altitudes.

The effective altitude range of the resonator can be estimated by studying how the modeled IAR effects on the ground will change when the IAR altitude range is varied. Fig. 5a shows a frequency dependence of the TC coefficient calculated for the average ionosphere discussed above (see Figs. 2c and 4). As earlier, we have assumed a planar L-mode wave incident upon the ionosphere with the local inclination angle of $\theta_{\parallel} = 66^{\circ}$. Here the maximum altitude of the CP-7 mode was used as the upper boundary for modeling and as the altitude of the incoming wave ($z_{max} = 2310$ km). Then the IAR resonances were located at about f_0~0.13, f_1~0.40, f_2~0.64, and f_3~0.89 Hz. Practically the same resonance frequencies were found when the wave incidence boundary was taken at $z_{max} = 1440$ km (see Fig. 5b).

Reducing the altitude range still further down to $z_{max} = 1210$ km results in the TC(f) spectrum shown in Fig. 5c. There the two lower resonances still remain at the same frequencies (f_0~0.13, f_1~0.40 Hz) but the higher harmonics are shifted

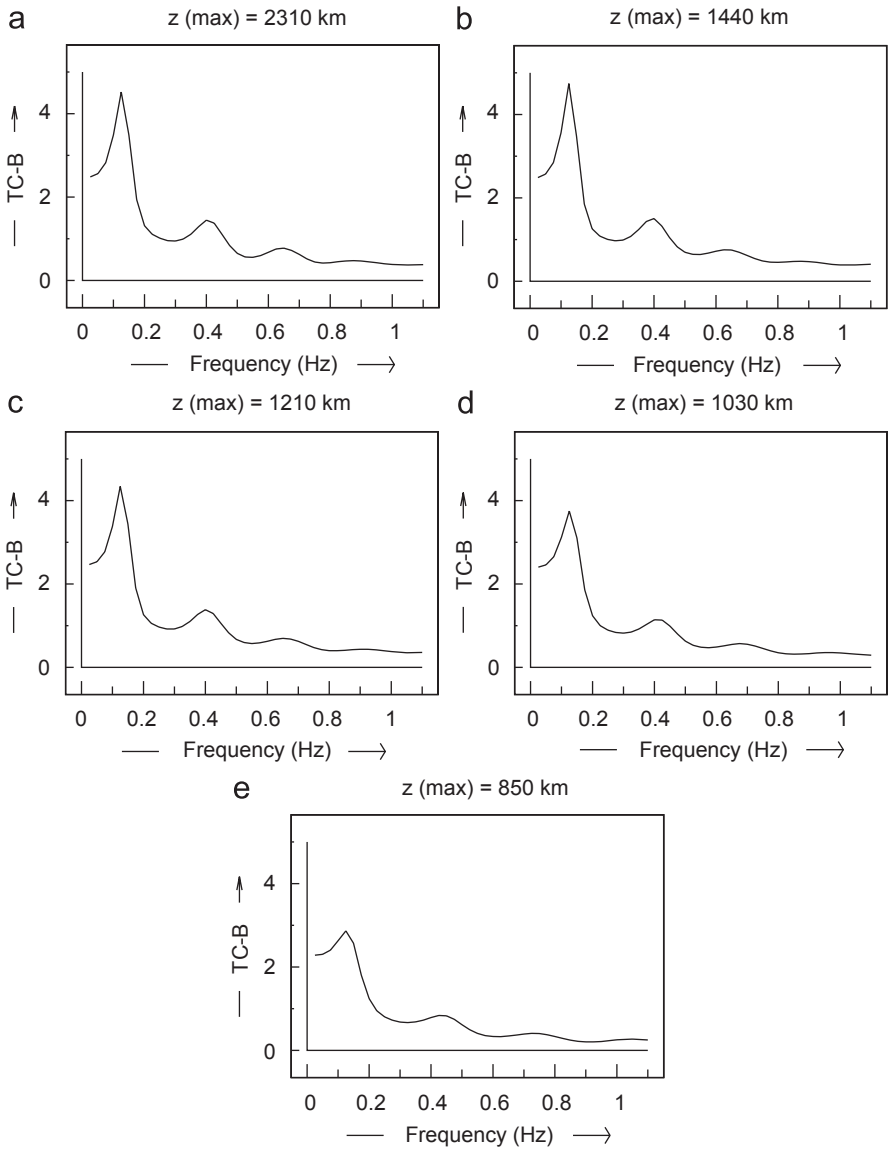

Fig. 5. TC(f)-spectra for the average ionosphere model (Fig. 4) with variable z_{max}. An $L_{\parallel}$-mode wave is assumed upon the ionospheric boundary at (a) $z_{max} = 2310$ km, (b) $z_{max} = 1440$ km, (c) $z_{max} = 1210$ km, (d) $z_{max} = 1030$ km, and (e) $z_{max} = 850$ km.

slightly higher to $f_2 \sim 0.66$ Hz and $f_3 \sim 0.91$ Hz. Thus, for the low-frequency EMIC (and other possible) wave bands whose frequencies are located around the two lowest IAR harmonics (typically below some 0.5 Hz), a 1200–1500 km thick ionosphere would be sufficient for a realistic modeling of the IAR effects.

Fig. 5d shows the TC(f) spectrum calculated in the case of a still lower upper boundary of $z_{max} = 1031$ km. Now, a small shift higher is also observed for the first harmonic whose peak is now at $f_1 \sim 0.41$ Hz. Accordingly, using a model ionosphere with (or ionospheric measurements over) an altitude range of about 1000 km or less may not be quite sufficient for a realistic modeling of waves whose frequency is located at the first harmonic f_1 (or above). Naturally, the second and third harmonics are also shifted upward, roughly to $f_2 \sim 0.69$ and $f_3 \sim 0.98$ Hz. A further decrease of the boundary to $z_{max} = 850$ km raises the resonance frequencies further up (e.g., $f_1 \sim 0.43$ Hz), as shown in Fig. 5e. We note that finding higher resonance frequencies for a shorter ionospheric cavity follows the general property of all resonators. Note also that, while reducing the altitude range of the ionosphere, the quality (Q value) of the resonator is also reduced and the IAR becomes sloppier.

3.3. IAR vertical structure

In order to obtain a better view of the structure and action of the IAR let us now study the vertical profile of the total horizontal magnetic field of the standing wave modeled using altitude steps of 10 km (see also Prikner et al., 2004). We have calculated the TC(f, z) function (Eq. (2)) for the first harmonic $f_1 \sim 0.40$ Hz using the averaged IAR model mentioned above. Fig. 6a shows the vertical profile of the full standing wave up to 2000 km assuming that an $L_{\|}$-mode wave with frequency $f_1 = 0.40$ Hz is incident upon the ionospheric boundary at $z_{max} = 2310$ km. The IAR includes two amplitude maxima, one at $z \approx 170$ km and the other at $z \approx 500$ km. After a minimum at about $z \approx 1000$ km the amplitude increases slowly but continuously up to the boundary of incidence z_{max} without attaining a maximum.

Fig. 6b shows the vertical profile of TC(f, z) for the case when the boundary of the wave incidence is reduced to $z_{max} = 1210$ km. The structure of the standing wave, the maxima, and the minima remain practically identical below the altitude of 1000 km,

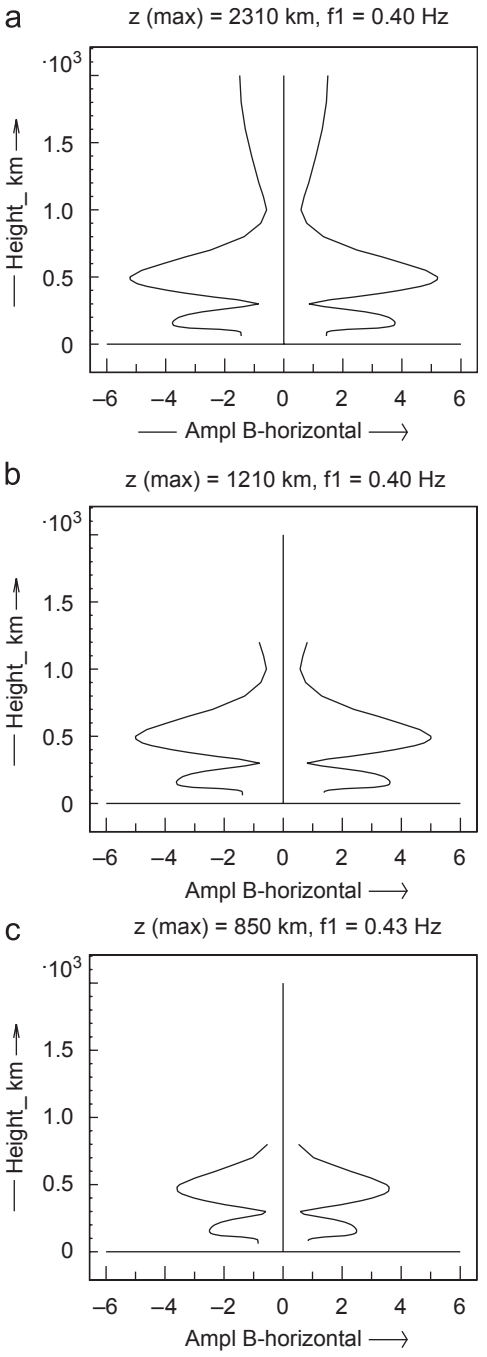

Fig. 6. Altitude profiles of the normalized amplitudes of the horizontal component B_h for the first harmonic f_1 using the average ionosphere model (Fig. 4) with variable z_{max}. (a) $z_{max} = 2310$ km, (b)$z_{max} = 1210$ km, and (c) $z_{max} = 850$ km.

at least at the altitude resolution of 10 km used here. Only the monotonic upper part has been cut off. However, the situation is different for the higher harmonics $f_r > f_1$ whose upper maxima are located

at higher altitudes than those of the lower harmonics (Prikner et al., 2004) and, therefore, are more vulnerable to be affected when reducing the effective IAR altitude. Thus, the higher harmonics of the IAR are expected to respond sooner and more dramatically to the reduction of the IAR altitude range than the lower harmonics. This is also the cause of the frequency increase of the higher harmonics $f_r > f_1$ in Figs. 5c–e.

Fig. 6c shows the vertical structure of the IAR standing wave for an even more reduced ionosphere where the incidence level is set to $z_{max} = 850$ km. As mentioned above (Fig. 5e), in this case the IAR was changed so much that even the first harmonic was shifted to a higher value $f_1 \sim 0.43$ Hz. The smaller vertical range decreases the wavelength of the standing wave and shifts the wave maxima to lower altitudes so that the lower maximum is found at $z \approx 160$ km and the upper maximum at $z \approx 460$ km. From this analysis we can conclude that, when modeling the IAR effect on waves in the Pc1 pulsation range, the required altitude range for the first few harmonics $f_r \leqslant f_3$ is between 1200 km and $< z_{max} \leqslant 1500$ km.

4. Summary and conclusions

4.1. IAR effect calculated using EISCAT high-altitude measurements

The ionospheric Alfvén resonator (IAR) is known to affect ground-based Pc1 (and other short-period ULF) wave activity. We have earlier modeled the IAR numerically using ionospheric data from low-altitude EISCAT measurements (operated, e.g., in CP-1 or CP-3 modes), which extend at most up to the altitude of 600 km. In order to obtain a realistic model we always had to extrapolate the measurements of the critical ionospheric parameters to higher altitudes (see, e.g., Prikner et al., 2001, 2002, 2004; Prikner and Kerttula, 2005). The EISCAT CP-7 mode offers the possibility to construct a more realistic ionospheric model, which allows confirming the IAR effect on the wave signal observed on the ground. Moreover, realistic IAR models can be utilized, e.g., when studying spectral resonance structures (Bösinger et al., 2002, 2004; Hebden et al., 2005), or as a support when comparing results from a modified ionosphere with theoretical considerations (see, e.g., Pilipenko et al., 2002).

The multiband waves observed at the Finnish subauroral KIL and IVA stations on March 7, 2001, showed a complicated time development. Most of the event around the local noon was observed by the simultaneously operated CP-1 and CP-7 modes of the EISCAT radar. This allowed constructing realistic vertical plasma profiles up to the altitude of 2300 km, suitable for the numerical IAR modeling. The IAR resonance structure on the ground was compared with the dynamic spectra of the waves observed at KIL and IVA. Despite rather large variations of plasma parameters in individual measurements, especially at high altitudes, we found a good correspondence between the observed wave frequencies on the ground and the modeled IAR resonance frequencies (TC-resonance peaks). This good correspondence supports the view that the IAR has an effect on the wave signal observed on the ground. Independently of the way of propagation (whether along the magnetic field line or along the horizontal waveguide) the wave signal can more easily reach the ground at the IAR eigenfrequencies. However, the IAR resonator is far from perfect and its effect is reduced at the higher harmonics where the quality of the resonator is lower. Accordingly, strong waves can penetrate the ionosphere even at frequencies outside the IAR eigenfrequencies, especially at higher frequencies, but the statistics of wave frequencies observed on ground is greatly affected by the IAR.

4.2. The effective IAR altitude range

The traditional view of the altitude range of the IAR is that it extends up to the (theoretical) Alfvén velocity maximum somewhere at the altitude of 2000–3000 km in the upper ionosphere at mid- to subauroral latitudes, and even higher at auroral latitudes. However, the main domain of the resonator is centered around the F2 layer density maximum. The required upper boundary of the IAR domain that is needed for an exact modeling can vary with the plasma conditions seasonally, daily, etc. With a multiband wave event with frequencies $f \leqslant 1$ Hz, we have demonstrated that a local maximum of the Alfvén velocity can exist in the ionosphere at an altitude below 2000 km (relative to the latitude observation studied). This reduces the effective altitude range of the IAR that is required when modeling the IAR resonances, especially the lower harmonics from the fundamental up to the second harmonic. We have shown that these resonances remain the same if the effective IAR range does not decrease

below $z_{max} \approx 1200$–1500 km. Also, the vertical profiles of the standing waves do not vary for these low harmonics if the IAR domain does not decrease below this z_{max} value. However, below this range the IAR eigenfrequencies shift higher and the vertical profiles of the standing wave are deformed, making numerical modeling unreliable. Accordingly, the effective IAR altitude range can be taken to extend up to the altitude of $z \approx 1200$–1500 km. These results apply specifically at mid- to subauroral latitudes. However, because of the different (and more variable) density profile and the higher altitude of the Alfvén speed maximum at auroral latitudes, the results may not directly apply there.

Acknowledgments

We acknowledge Prof. Emer. J. Kangas for discussions. K.P. thanks J. Manninen and J. Kultima (Sodankylä Observatory) for magnetic data, R. Kuula (Department of Physical Sciences, Oulu University) for EISCAT data and National Space Science Data Center (NSSDC, Greenbelt, MD 20771) for IRI models. K.P. also acknowledges the financial support of the EU's 5th Frame Programme under the IHP Programme (Contract HPRI200100132). F.Z.F. acknowledges the financial support by the Commission of the European Union (research grant INTAS), the Russian Fund for Basic Research, research Grants nos. 05-05-64992 and 06-05-65174, and the Program of Russian Academy of Sciences no. 16 "Solar activity and physical processes in the Solar–Earth system". The EISCAT Scientific Association is supported by the Suomen Akatemia of Finland, Centre National de la Recherche Scientifique, France, Max-Planck Gesellschaft, Federal Republic of Germany, National Institute of Polar Research of Japan, Norges Almenvitenskapelige Forskningsrad of Norway, Naturvetenskapliga Forskningsradet of Sweden, and the Science and Engineering Research Council of the United Kingdom.

References

Bösinger, T., Haldoupis, C., Belyaev, P.P., Yakunin, M.N., Semenova, N.V., Demekhov, A.G., Angelopoulos, V., 2002. Spectral properties of the ionospheric Alfvén resonator observed at a low-latitude station ($L = 1.3$). Journal of Geophysical Research 107 (A10), 1281 SIA4 (1–9).

Bösinger, T., Demekhov, A.G., Trakhtengerts, V.Y., 2004. Fine structure in ionospheric Alfvén resonator spectra observed at low latitude ($L = 1.3$). Geophysical Research Letters 31, L18802, (1–5).

Cummings, W.D., O'Sullivan, R.J., Coleman Jr., P.J., 1969. Standing Alfvén waves in the ionosphere. Journal of Geophysical Research 74, 778–793.

Fatkullin, M.N., Zelenova, T.I., Kozlov, V.K., Legenka, A.D., Soboleva, T.N., 1981. Empirical Models of the Mid-Latitude Ionosphere. Nauka, Moscow (in Russian).

Feygin, F.Z., Nekrasov, A.K., Kangas, J., Pikkarainen, T., 1994. Coherent multiple Pc1 pulsation bands: possible evidence for the ionospheric Alfvén resonator. Annales de Geophysicae 12, 147–151.

Greifinger, C., Greifinger, P., 1968. Theory of hydromagnetic propagation in the ionospheric waveguide. Journal of Geophysical Research 73, 7473–7490.

Hebden, S.R., Robinson, T.R., Wright, D.M., Yeoman, T.K., Raita, T., Bösinger, T., 2005. A quantitative analysis of the diurnal evolution of ionospheric Alfvén resonator magnetic resonance features and calculation of changing IAR parameters. Annales de Geophysicae 23, 1711–1721.

Kozyra, J.U., Cravens, T.E., Nagy, A.F., Fontheim, E.G., Ong, R.S.B., 1984. Effects of energetic heavy ions on electromagnetic ion cyclotron wave generation in the plasmapause region. Journal of Geophysical Research 89, 2217–2233.

Lysak, R.L., 1999. Propagation of Alfvén waves through the ionosphere: dependence on ionospheric parameters. Journal of Geophysical Research 104 (A5), 10017–10030.

Mursula, K., Prikner, K., Feygin, F.Z., Bräysy, T., Kangas, J., Kerttula, R., Pollari, P., Pikkarainen, T., Pokhotelov, O.A., 2000. Non-stationary Alfvén resonator: new results on Pc1 pearls and IPDP events. Journal of Atmospheric and Solar-Terrestrial Physics 62, 299–309.

Pilipenko, V.A., Fedorov, E.N., Engebretson, M.J., 2002. Alfvén resonator in the topside ionosphere beneath the auroral acceleration region. Journal of Geophysical Research 107 (A9), 1257 SMP21 (1–10).

Prikner, K., 1986. The ionosphere of higher geomagnetic latitudes ($L = 3$ and $L = 5$) as a ULF wave filter. Studia Geophysica et Geodaetica 30, 304–319.

Prikner, K., Kerttula, R., 2005. O^+-reduced models of the high latitude ionosphere and the ionospheric Alfvén resonator in broadband Pc1 events. Studia Geophysica et Geodaetica 49, 127–139.

Prikner, K., Vagner, V., 1991. Numerical solution to the problem of ionospheric filtration of ULF waves in the Pc1 range. The total wave field inside the ionospheric transition layer. Studia Geophysica et Geodaetica 35, 90–99.

Prikner, K., Mursula, K., Kangas, J., Feygin, F.Z., 2001. Ionospheric Alfvén resonator control over the frequency variable Pc1 event in Finland on May 14, 1997. Studia Geophysica et Geodaetica 45, 363–381.

Prikner, K., Mursula, K., Kangas, J., Feygin, F.Z., Kerttula, R., 2002. Numerical simulation of the high-latitude non-stationary ionospheric Alfvén resonator during an IPDP event. Studia Geophysica et Geodaetica 46, 507–526.

Prikner, K., Mursula, K., Kangas, J., Kerttula, R., Feygin, F.Z., 2004. An effect of the ionospheric Alfvén resonator on multiband Pc1 pulsations. Annales de Geophysicae 22, 643–651.

Young, D.T., Perraut, S., Roux, A., de Villedary, C., Gendrin, R., Korth, A., Kremser, G., Jones, D., 1981. Wave–particle interactions near O_{He+} observed on GEOS 1 and 2. 1. Propagation of ion cyclotron waves in He^+-rich plasma. Journal of Geophysical Research 86, 6755–6772.